Analytic solution for the critical state in superconducting elliptic films

Grigorii P. Mikitik
B. Verkin Institute for Low Temperature Physics & Engineering, National Ukrainian Academy of Sciences, Kharkov 310164, Ukraine

Ernst Helmut Brandt
Max-Planck-Institut für Metallforschung, D-70506 Stuttgart, Germany
(Received 8 February 1999)

A thin superconductor platelet with elliptic shape in a perpendicular magnetic field is considered. Using a method originally applied to circular disks, we obtain an approximate analytic solution for the two-dimensional critical state of this ellipse. In the limits of the circular disk and the long strip this solution is exact, i.e., the current density is constant in the region penetrated by flux. For ellipses with arbitrary axis ratio the obtained current density is constant to typically 10^{-3}, and the magnetic moment deviates by less than 10^{-3} from the exact value. This analytic solution is thus very accurate. In increasing applied magnetic field, the penetrating flux fronts are approximately concentric ellipses whose axis ratio $b/a \leqslant 1$ decreases and shrinks to zero when the flux front reaches the center, the long axis staying finite in the fully penetrated state. Analytic expressions for these axes, the sheet current, the magnetic moment, and the perpendicular magnetic field are presented and discussed. This solution applies also to superconductors with anisotropic critical current if the anisotropy has a particular, rather realistic form. [S0163-1829(99)04825-0]

I. INTRODUCTION

Most experiments with high-T_c superconductors deal with thin flat samples in a perpendicular magnetic field H, for example, c-axis-oriented monocristalline platelets or films. In this connection, in recent years the problem of the critical state of such samples has attracted considerable interest, see, e.g., Ref. 1, and the references cited therein. Exact analytic solutions were obtained only for a circular disk[2] and a thin infinitely long strip.[3–5] In deriving these solutions it was essential that the critical states of the disk and the strip have a known symmetry. For the strip the critical-state distributions of the magnetic field and the current do not depend on the longitudinal coordinate while the disk has a rotational axis. In both cases the directions of circulating currents are fixed and known in advance, and thus the critical-state equations are one-dimensional (1D). In the present paper we obtain an approximate analytic solution of a two-dimensional (2D) problem, namely, a thin superconductor platelet of elliptic shape in a perpendicular magnetic field. This solution enables one to understand the critical states of real superconductors when the above-mentioned symmetry is absent. The accuracy of our solution is very high, especially for the integral quantities like the magnetization of the sample, and it may be used to analyze experimental data. Besides this, the analysis of our solution reveals qualitatively new features of the critical state of thin superconductors like flux fronts with varying curvature and the possibility of rotating flux-line arrangments.

We derive this solution in Sec. II and analyze it in Sec. III, reproducing the known solutions for disks and strips and discussing the interesting new features. In Sec. IV we apply our solution to anisotropic superconductors, and in Sec. V we summarize the results.

II. DERIVATION

Let us place the origin of the coordinate system in the center of the sample and let its plane coincide with the xy plane. The external magnetic field H is directed along the z axis, i.e., along the thickness d of the sample. The boundary of the superconductor in the xy plane Γ is described by the ellipse (see Fig. 1)

$$\frac{x^2}{a_0^2}+\frac{y^2}{b_0^2}=1,$$

where a_0 and b_0 are the semiaxes of the ellipse ($a_0 \geqslant b_0 \gg d$). The critical current density j_c is assumed to be constant. The critical-state equations for the thickness-integrated current density $\mathbf{J}(x,y)=\int_{-d/2}^{d/2}\mathbf{j}(x,y,z)dz$ in the partly penetrated critical state have the following form. In the region between Γ and the penetrating flux front γ one has

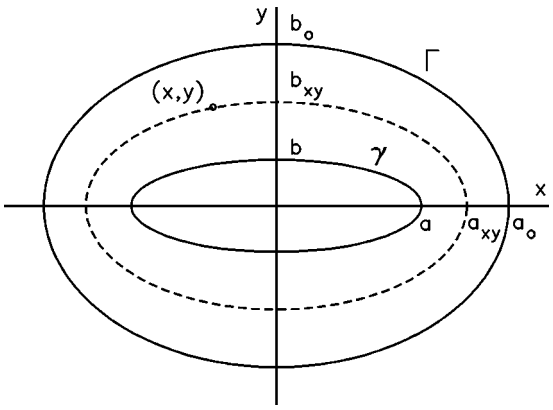

FIG. 1. The three ellipses defining the edge Γ of the film with semiaxes a_0, b_0; an earlier flux front passing through a given point (x,y) (semiaxes a_{xy}, b_{xy}, dashed line); and the present flux front with semiaxes a, b.

$$|\mathbf{J}(x,y)| = j_c d \equiv J_c . \tag{1}$$

Here the common assumption has been made that the direction of the current does not depend on the coordinate z across the small thickness of the sample. In the flux-free region, i.e., inside γ, the perpendicular induction should vanish,

$$B_z(x,y) = 0. \tag{2}$$

In addition, the equation

$$\nabla \cdot \mathbf{J}(x,y) = 0 \tag{3}$$

must hold for any x and y inside the sample. In deriving the solution we follow the method of Mikheenko and Kuzovlev.[2] When γ coincides with Γ, i.e., the flux does not penetrate the superconductor, the solution of Eqs. (2) and (3) may be found by considering the field on the surface of an ideally screening oblate ellipsoid in a uniform magnetic field $H \| z$. The field at the surface of the ellipsoid is tangential to it and has the form[6]

$$\mathbf{H}_t(x,y,z) = \frac{H}{1-N_{zz}} [\hat{\mathbf{z}} - \hat{\mathbf{n}}(\hat{\mathbf{z}}\hat{\mathbf{n}})].$$

Here $\hat{\mathbf{z}}$ is the unit vector along z, $\hat{\mathbf{n}}$ is the unit vector normal to the surface, and N_{zz} is the appropriate demagnetizing factor. For a thin oblate ellipsoid with semiaxes $a_0 \geqslant b_0 \gg c_0$ one has[7] $1-N_{zz} = (c_0/b_0)E(k)$ where $E(k)$ is the complete elliptic integral of the second kind with $k^2 = 1 - b_0^2/a_0^2$. For example, when $a_0 = b_0$ (disk) one has $E(0) = \pi/2$ and $1 - N_{zz} = \pi c_0/2a_0$, and when $a_0 \gg b_0$ (strip) one has $E(1) = 1$ and $1 - N_{zz} = c_0/b_0$. Letting $c_0 \to 0$ and taking into account the relation between the surface screening current and the tangential field, $\mathbf{J}_{\rm surf} = \hat{\mathbf{n}} \times \mathbf{H}_t$,[6] we arrive at the sheet current

$$\mathbf{J}(x,y) = 2\hat{\mathbf{z}} \times \mathbf{H}_t ,$$

where $\mathbf{H}_t$ is the field on the upper side of the platelet. This result applies to films of any shape; it means that the magnitude of the field change across the film thickness equals J. In thin ellipses, in the region $f(x/a_0, y/b_0) < 1$ with $f(u,v) \equiv u^2 + v^2$, one obtains for $\mathbf{J} = (J_x, J_y)$:

$$J_x = \frac{2H}{E(k)} \frac{y}{b_0} \; S \equiv -HF_x\left(\frac{x}{a_0}, \frac{y}{b_0}, \frac{b_0}{a_0}\right),$$

$$J_y = -\frac{2H}{E(k)} \frac{x b_0}{a_0^2} S \equiv -HF_y\left(\frac{x}{a_0}, \frac{y}{b_0}, \frac{b_0}{a_0}\right), \tag{4}$$

where $S = 1/\sqrt{1 - x^2/a_0^2 - y^2/b_0^2}$ and $k^2 = 1 - (b_0/a_0)^2$. If $f(x/a_0, y/b_0) > 1$, we define $F_x = F_y = 0$. When a partially penetrated critical state occurs in the sample, we look for the solution of Eqs. (1), (2), (3) as a linear combination of distributions like that described by formulas (4). In other words, we assume that the front of flux penetration has the shape of an ellipse with the ratio of the semiaxes depending on the depth of the penetration, see Fig. 1. This assumption is exact for disks and strips and also in the limiting case of a small depth of penetration. As will be seen from the results obtained below, the deviation from this assumption increases with increasing depth but remains very small. The proposed approximation thus is sufficient for most practical purposes.

Let the penetrating flux front be the ellipse

$$f\left(\frac{x}{a(b)}, \frac{y}{b}\right) = 1 \tag{5}$$

with the long axis a depending on the short axis b. Then, according to the above assumption, we write for the components J_x and J_y of the sheet current,

$$J_{x,y} = -H \int_b^{b_0} W(b') F_{x,y}\left(\frac{x}{a(b')}, \frac{y}{b'}, \frac{b'}{a(b')}\right) db', \tag{6}$$

where $W(b')$ is a weight function and F_x and F_y are defined by Eqs. (4). The sheet current (6) with any weight $W(b')$ satisfies Eq. (3) due to the definition of the functions F_x and F_y. In the elliptic region

$$f\left(\frac{x}{a(b)}, \frac{y}{b}\right) < 1$$

and this current creates a constant field equal to

$$-H \int_b^{b_0} W(b') db',$$

which has to compensate the applied field H. Thus, condition (2) reduces to the equation

$$\int_b^{b_0} W(b') db' = 1. \tag{7}$$

The functions $W(b)$ and $a(b)$ must be obtained from the equality

$$J_x^2 + J_y^2 = J_c^2 , \tag{8}$$

which follows from Eq. (1). Let $x = 0$. Then Eq. (8) takes the form which was considered in Ref. 2, and we find

$$W(b) = \frac{J_c}{\pi H} \frac{E(k)}{b\sqrt{1 - b^2/b_0^2}} \tag{9}$$

with $k^2 = 1 - [b/a(b)]^2$. Now we can obtain the function $J_x(x=0,y)$ [while $J_y(x=0,y) = 0$] and calculate the total current I circulating in the sample,

$$I = \int_0^{b_0} J_x(0,y) dy = \frac{2}{\pi} J_c b_0 \arccos\frac{b}{b_0}. \tag{10}$$

The H dependence of the penetration depth $b(H)$ along the y axis is determined by Eq. (7). This yields

$$\frac{H}{H_c} = \int_b^{b_0} \frac{E(k) db'}{b'\sqrt{1 - b'^2/b_0^2}} \tag{11}$$

with $H_c \equiv J_c/\pi \equiv j_c d/\pi$ and $k^2 = 1 - [b'/a(b')]^2$, see Fig. 2. To determine the dependence $a(b)$ let us repeat the above reasoning, Eqs. (5)–(10), but now we shall consider b as a function of a and integrate over a' from a to a_0. At $y = 0$ we can find $W(a')$ and calculate I again, obtaining

$$I = -\int_0^{a_0} J_y(x,0) dx = \frac{2}{\pi} J_c a_0 \arccos\frac{a}{a_0}. \tag{12}$$

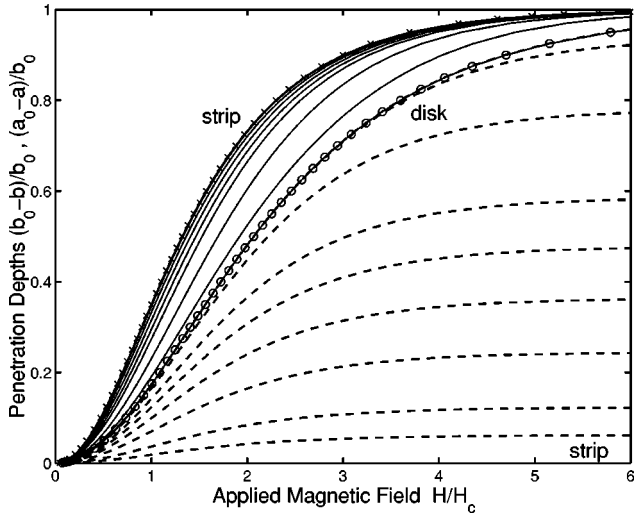

FIG. 2. The semiaxes a and b of the elliptic flux fronts plotted as reduced penetration depths $(a_0-a)/b_0$ (dashed lines) and $(b_0-b)/b_0$ (solid lines) versus the applied field H (in units of $H_c=J_c/\pi$) for thin ellipses with eccentricities $e=b_0/a_0=$ 1, 0.9, 0.7, 0.5, 0.4, 0.3, 0.2, 0.1, 0.05, 0. The curve for the disk [$e=1$, $a=b$, Eq. (20) with H_c replaced by $J_c/2$] is marked by circles. For strips, b [Eq. (20)] is marked by crosses, and one has $a_0-a=0$.

Since the total current crossing any radius must be the same, we may equate the currents (10) and (12). This yields the dependence of a on b (Fig. 3),

$$a(b)=a_0\cos\left(\frac{b_0}{a_0}\arccos\frac{b}{b_0}\right). \tag{13}$$

Formulas (4)–(6), (9), (11), and (13) give the solution for the critical state in the ellipse. If this solution were exact, Eq. (8) would hold for any x and y in the region between the curves Γ and γ. The numerical analysis shows that, in reality, the quantity $\tilde{J}\equiv(J_x^2+J_y^2)^{1/2}/J_c$ gradually deviates from 1 as the point (x,y) moves away from Γ. However, this deviation remains small, typically 10^{-4}–10^{-2}, and is not visible in

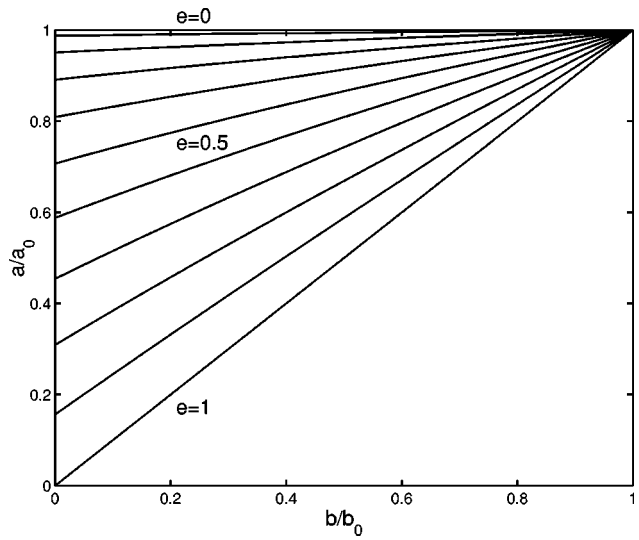

FIG. 3. The long semiaxis a as function of the short semiaxis b of the penetrating elliptic flux front for various eccentricities $e=b_0/a_0=$ 1, 0.9, 0.8, . . . , 0.1, 0, Eq. (13).

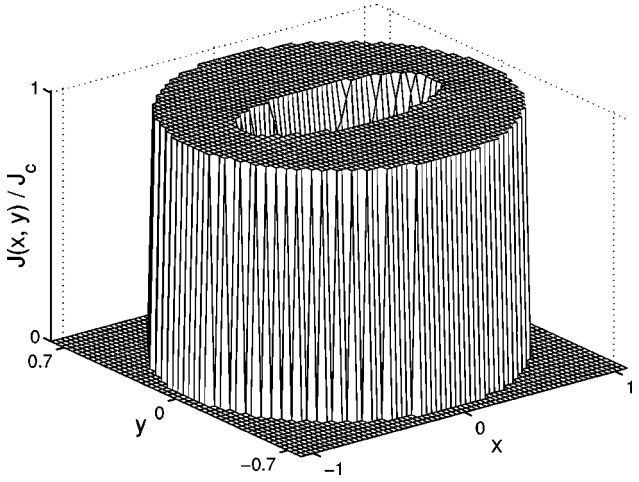

FIG. 4. 3D plot of the magnitude of the sheet current $|\mathbf{J}(x,y)|$, Eq. (19), in a thin ellipse with $b_0/a_0=0.7$ at $b/a_0=0.2$. In the flux-penetrated region the plotted J/J_c deviates from unity by less than 10^{-3}.

Figs. 4–7. In the fully or almost fully penetrated state near the points $x=\pm a(b=0)$, $y=0$, this deviation may reach a few percent. Our expressions provide thus a very good description of the critical state in elliptic platelets. In particular, since this small deviation of $J(x,y)$ from J_c occurs mainly near the axis $y=0$, its influence on the magnetic moment will be negligible, see Sec. III.

Interestingly, an explicit expression can be obtained for the b dependence of the magnetic moment m of our elliptic disk in the critical state. In the ideal screening state any ellipsoid with volume V and semiaxes a_0,b_0,c_0 in a field $H\|z$ has the magnetic moment

$$m_{\rm ideal}(a_0,b_0,c_0)=-\frac{VH}{1-N_{zz}}=-\frac{4\pi}{3}\frac{a_0b_0c_0}{1-N_{zz}}H.$$

For thin oblate ellipsoids with $a_0\geqslant b_0\gg c_0$ the demagnetizing factor is[7] $N_{zz}=1-(c_0/b_0)E(k)$ with $k^2=1-b_0^2/a_0^2$. Taking

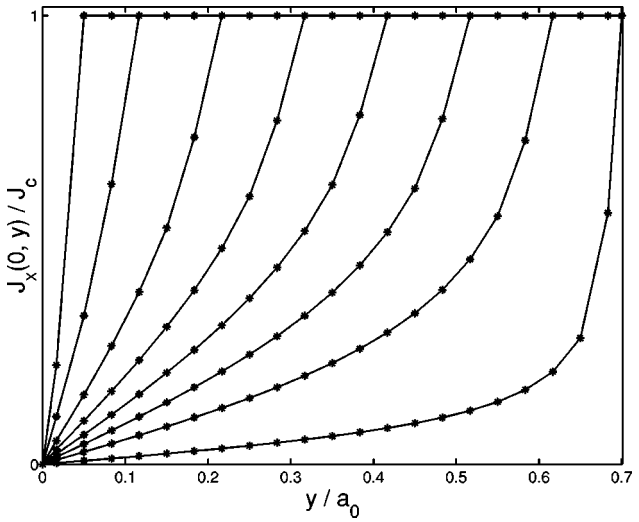

FIG. 5. Profiles of the sheet current $J_x(0,y)$ in a thin ellipse with $b_0/a_0=0.7$ for various degrees of flux penetration $b/a_0=$ 0.69, 0.6, 0.5, . . . , 0.1, 0.05 (from right to left). Note the precise saturation to $J=J_c$, which demonstrates the accuracy of our approximation.

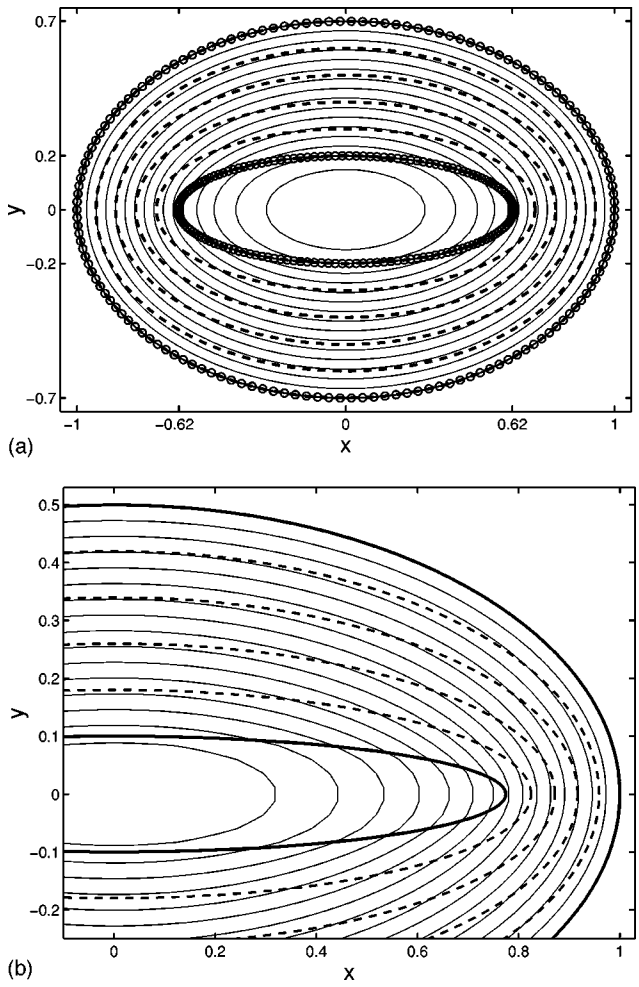

FIG. 6. Stream lines (solid lines) of the sheet current $\mathbf{J}(x,y)$ in a thin ellipse with (a) $b_0/a_0=0.7$, $b/a_0=0.2$ (yielding $a=0.624$) and (b) $b_0/a_0=0.5$, $b/a_0=0.1$ (yielding $a=0.775$). Also shown are five previous flux fronts (dashed lines) at equidistant values of b. The edge of the film and the inner flux front are indicated by circles and a bold line. Note that in general the sheet current does not flow parallel to the flux fronts and that its magnitude is constant in the flux-penetrated region.

the limit $c_0\rightarrow 0$ one obtains the magnetic moment of an ideally screening thin ellipse,

$$m_{\mathrm{ideal}}(a_0,b_0)=-\frac{4\pi}{3}\frac{a_0 b_0^2}{E(k)}H. \tag{14}$$

For the thin ellipse in the critical state we write

$$m=\int_b^{b_0} W(b')m_{\mathrm{ideal}}[a(b'),b']db'. \tag{15}$$

With the weight (9) the elliptic integral $E(k)$ drops out and this integral yields

$$m=-\frac{2}{3}J_c a_0 b_0^2\left[\frac{\cos(\arcsin\tilde{b}+e\arccos\tilde{b})}{1-e}+\frac{\cos(\arcsin\tilde{b}-e\arccos\tilde{b})}{1+e}\right], \tag{16}$$

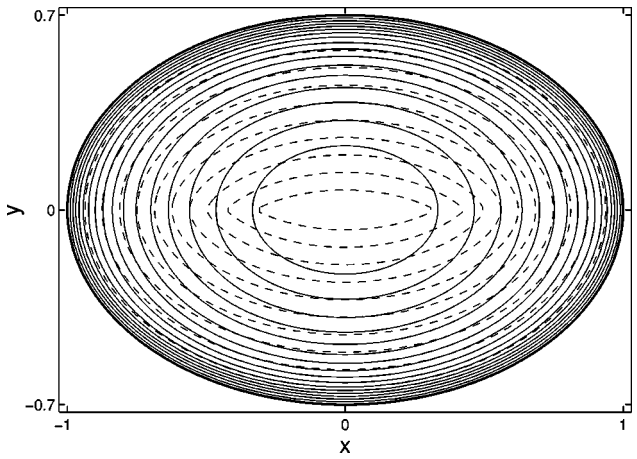

FIG. 7. The stream lines of the sheet current in the same ellipse ($b_0/a_0=0.7$) at two different times during flux penetration: at $b/a_0=0.65$ (solid lines, almost ideal screening) and $b/a_0=0.01$ (dashed lines, almost full penetration). Note that the orientation of the sheet current at some places changes strongly during the penetration, leading to a rotating vortex arrangment across the thickness of the film.

where $e=b_0/a_0$ and $\tilde{b}=b/b_0$. The dependence $m(H)$ is obtained from Eqs. (11) and (16), see Fig. 8.

Next we give the expression for the magnetic field $H_z(x,y)$ in the penetrated region between Γ and γ. Let the point (x,y) be located on the ellipse

$$\frac{x^2}{a_{xy}^2}+\frac{y^2}{b_{xy}^2}=1 \tag{17}$$

with semiaxes a_{xy} and b_{xy}, where $b\leqslant b_{xy}\leqslant b_0$ and $a_{xy}=a(b_{xy})$ satisfies Eq. (13), i.e., the ellipse is a previous flux front, Fig. 1. Then we obtain

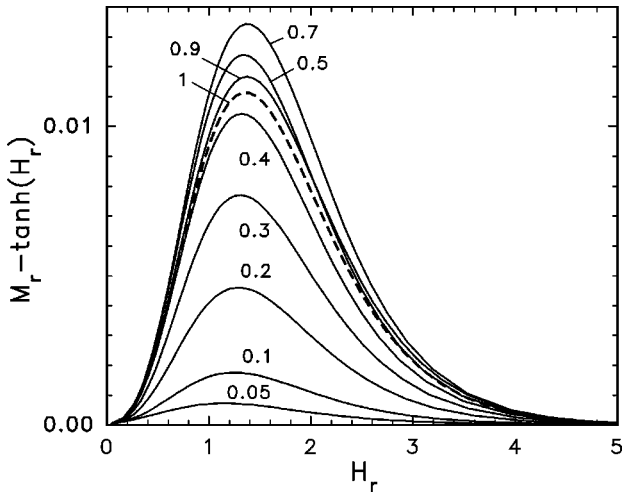

FIG. 8. The magnetic moment (magnetization curve) of thin ellipses in a perpendicular magnetic field in the Bean model, plotted in normalized form as deviation from the strip result $M_r=\tanh(H_r)$ versus a reduced field $H_r=H/H_1$ for eccentricities $e=b_0/a_0=$ 1, 0.9, 0.7, 0.5, 0.4, 0.3, 0.2, 0.1, and 0.05, see Eqs. (11), (16), and (24)–(26).

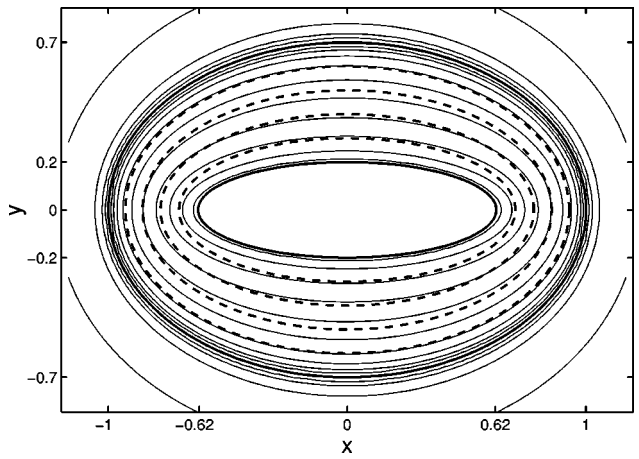

FIG. 9. Contour lines (solid lines) of the perpendicular magnetic field $H_z(x,y)$ of a thin ellipse with $b_0/a_0=0.7$ in the plane $z=0$ for partial flux penetration with $b/a_0=0.2$, as in Fig. 6(a). Note that these contours are nearly parallel to the elliptic flux fronts shown as dashed lines for $b/a_0=0.7$, 0.6, 0.5, 0.4, 0.3, and 0.2. The edge of the specimen and the inner flux front are marked by bold lines. Inside the inner flux front one has exactly $H_z(x,y)=0$.

$$H_z(x,y)=H_c\int_b^{b_{xy}}\frac{db'}{\sqrt{1-b'^2/b_0^2}}\times\left\{\frac{b'}{a(b')}\sqrt{\frac{\xi+a^2(b')}{\xi(\xi+b'^2)}}+\frac{E(\varphi,k)}{b'}\right\}. \quad (18)$$

Here $E(\varphi,k)$ is the elliptic integral of the second kind, $\sin\varphi=[\xi/(\xi+b'^2)]^{1/2}$, $k^2=1-[b'/a(b')]^2$, and

$$2\xi=x^2+y^2-a'^2-b'^2+[(x^2+y^2-a'^2-b'^2)^2-4(b'^2a'^2-x^2b'^2-y^2a'^2)]^{1/2}$$

with $a'=a(b')$ from Eq. (13). The magnetic field outside the superconductor in the $z=0$ plane is given by the same expression (18) but with the upper boundary b_{xy} replaced by b_0, and inside the flux front γ one has $H_z=0$, see the Appendix. Contour lines and profiles of $H_z(x,y)$ are depicted in Figs. 9–11. At large distances $r=(x^2+y^2)^{1/2}\gg a_0\geqslant b_0$ the field (18) becomes

$$H_z(x,y)\to H-m/(4\pi r^3),$$

as expected,[6] with magnetic moment m from Eq. (16).

To end this section we give an elegant representation of the sheet current $\mathbf{J}(x,y)$. Substituting Eqs. (4) and (9) into Eq. (6), the expression for the components J_x and J_y can be written as follows:

$$J_x=J_c\frac{\partial g}{\partial y},\quad J_y=-J_c\frac{\partial g}{\partial x},$$

$$g(x,y)=-\frac{2}{\pi}\int_{b_{xy}}^{b_0}\frac{db'}{\sqrt{1-b'^2/b_0^2}}\sqrt{1-\frac{x^2}{a^2(b')}-\frac{y^2}{b'^2}}. \quad (19)$$

As in Eq. (18) the boundary b_{xy} is the semiaxis of a previous flux front defined by Eq. (17) if the point (x,y) is located between the curves Γ and γ, and $b_{xy}=b$ when the point is inside γ (in the field-free core). For points outside the superconductor we set $b_{xy}=b_0$, yielding $g=0$. The function $g(x,y)$ is the local magnetization (or density of current loops) introduced in Ref. 8; the contour lines $g(x,y)=$const coincide with the current stream lines; one has $g(x,y)=0$ on the edge Γ of the elliptic sample (and outside), and the volume under the ''mountain'' $g(x,y)$, coincides with the magnetic moment (16). We emphasize that the current stream lines in the general ellipse are *not parallel* to the flux front γ, see Fig. 6, in contrast to the situation in thin disks and strips, and in longitudinal geometry.

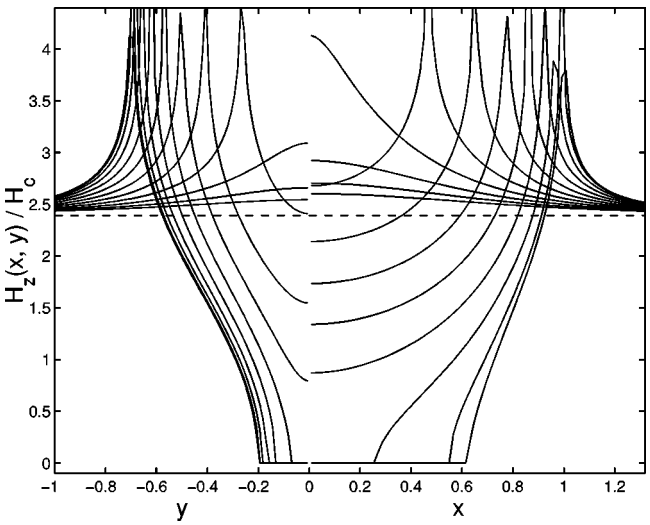

FIG. 10. Profiles of the magnetic field $H_z(x,y)$ of Fig. 9 plotted along y (left) and along x (right) for discrete equidistant values of x or y, respectively. The dashed line marks the applied field $H/H_c=2.39$.

III. ANALYSIS

One easily verifies that the obtained expressions for the penetration depth, Eq. (11), the magnetic field, Eq. (18), and the currents, Eq. (19), go over into the appropriate formulas for the disk[2] when $a_0=b_0$ and for the strip[3–5] when $a_0\gg b_0$.

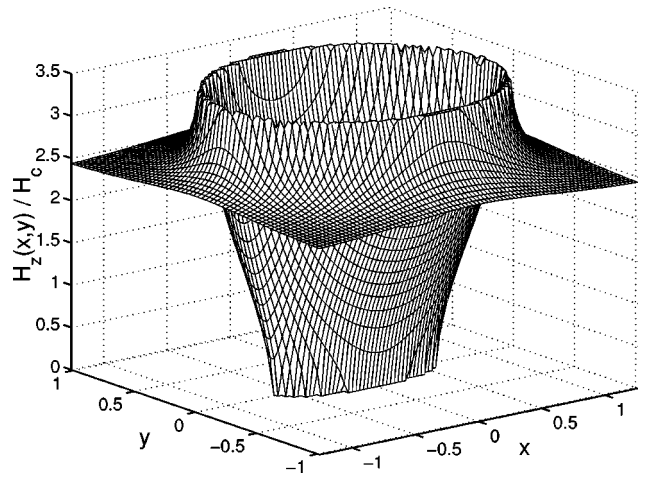

FIG. 11. 3D plot of the magnetic field $H_z(x,y)$ for $b_0/a_0=0.7$ and $b/a_0=0.2$ as in Figs. 9 and 10. The logarithmic infinity at the edge of the ellipse is cut off at $H_z/H_c=3.5$ to limit the irregular peaks caused by the equidistant grid used for this plot.

For the strip one has $E(k=1)=1$ and formula (11) yields the flux-front position

$$\frac{b}{b_0}=\frac{1}{\cosh(H/H_c)}, \tag{20}$$

which coincides with Eq. (3.5) of Ref. 4 since $H_c=J_c/\pi$. For the disk, $E(k=0)=\pi/2$ and we arrive at the same expression (20) but with H_c substituted by $\pi H_c/2=J_c/2$, see Eq. (19) of Ref. 2. For general ellipses, $b(H)$ falls between the curves for the disk and the strip, see Fig. 2. It should be noted that the penetration along the x axis does not go all to the center but $a(b)$ Eq. (13) approaches the finite value $a(0)=a_0\cos(\pi e/2)$ when $b\to 0$.

As for the magnetic moment, when $a_0=b_0$ Eq. (16) goes over to the appropriate formula for disks,[2]

$$m_{\rm disk}=-\frac{2}{3}J_c a_0^3\left(\arccos\frac{1}{\cosh h}+\frac{\sinh|h|}{\cosh^2 h}\right) \tag{21}$$

with $h=2H/J_c$. In the limit $a_0\gg b_0$, Eq. (16) yields the magnetic moment of strips with width $2w$ and length $2a_0$,

$$m_{\rm strip}=-2J_c a_0 w^2\tanh(H/H_c), \tag{22}$$

with an effective width $2w=(2/3)^{1/2}2b_0$. This $m_{\rm strip}$ deviates from the result for a strip with width $2b_0$ by a factor 2/3. The reduced effective width is explained as follows. A long narrow ellipse with semiaxes $a_0\gg b_0$ at each position x may be approximated by a piece of a long strip with half width $y(x)$, having a magnetic moment proportional to $y^2(x)/b_0^2=1-x^2/a_0^2$, cf. Eq. (22). Averaging this prefactor over the length $2a_0$ of the ellipse one arrives at the reduction factor 2/3.

The magnetization curves $m(H)$ for disks (21), strips (22), and the general ellipse, Eqs. (16) and (11), coincide almost exactly when they are normalized such that their initial slope and saturation value are unity. The deviation of these reduced curves $M_r(H_r)$ from the strip result $\tanh(H_r)$ are always smaller than 0.013 as shown in Fig. 8. The maximum deviation occurs for ellipses with eccentricity $e=b_0/a_0\approx 0.7$. Taking the initial slope $m'(0)=\partial m/\partial H|_{H=0}$ from Eq. (14),

$$m'(0)=\frac{m_{\rm ideal}}{H}=-\frac{4\pi}{3}\frac{a_0 b_0^2}{E(k)}, \tag{23}$$

($k^2=1-e^2$, $e=b_0/a_0$), and the saturation value $m_{\rm sat}=m(H\to\infty)$ from Eq. (16),

$$m_{\rm sat}=m(b\to 0)=-\frac{4}{3}J_c a_0 b_0^2\frac{\cos(e\pi/2)}{1-e^2}, \tag{24}$$

and approximating the normalized curves by $M_r(H_r)=\tanh(H_r)$ with $M_r=m/m_{\rm sat}$ and $H_r=H/H_1$,

$$H_1=\frac{m_{\rm sat}}{m'(0)}=J_c\frac{E(k)}{\pi}\frac{\cos(e\pi/2)}{1-e^2}, \tag{25}$$

we get an excellent approximation for the magnetic moment of thin ellipses in the Bean model,

$$m(H)\approx m_{\rm sat}\tanh(H/H_1), \tag{26}$$

with $m_{\rm sat}$ and H_1 from Eqs. (24) and (25). Formula (26) is good also for rectangular films, where $m_{\rm sat}$ is well known and $m'(0)$ has to be obtained numerically using the method of Ref. 9.

The sheet current **J**, Eqs. (6) and (19), reduces to the known results for circular disks[2] and infinite strips.[3–5] In both limits one obtains the same functional form for the magnitudes $J(r)=J_c f(r)$ and $J(y)=J_c f(y)$, with the same function: $f(y)=1$ for $b\leqslant|y|\leqslant b_0$ and

$$f(y)=\frac{2}{\pi}\arctan\frac{cy}{\sqrt{b^2-y^2}} \tag{27}$$

for $|y|\leqslant b$, where $c=(1-b^2/b_0^2)^{1/2}=\tanh(h)$ with $h=2H/J_c$ for the disk and $h=\pi H/J_c$ for the strip. For long ellipses with finite length $2a_0$ in these expressions b_0 should be replaced by the effective half width $y(x)$ as discussed after Eq. (22).

There is another known result with which our solution may be compared. Namely, in the flux-penetrated region where $J=J_c$ is constant, the current stream lines are equidistant and are thus the ''distance function.''[10] This means all points on a given stream line have the same distance from the specimen edge. This property applies to thin films of *any* shape. It applies also in the longitudinal geometry, i.e., in both limits of small and large thickness. (In the nonpenetrated region the current stream lines are different in these two limits: in the longitudinal limit one has there $j\equiv 0$ and $J\equiv 0$, but in the transverse limit $J\neq 0$). The current stream lines in the penetrated region are thus the envelope lines of circles with constant radius r ($0\leqslant r\leqslant b_0-b$) and with center on the specimen edge. Parametrizing our elliptic edge by $x(\varphi)=a_0\cos\varphi$, $y(\varphi)=b_0\sin\varphi$, we find for these envelopes

$$x(\varphi,r)=(a_0-rb_0/W)\cos\varphi,$$

$$y(\varphi,r)=(b_0-ra_0/W)\sin\varphi, \tag{28}$$

with $W=(b_0^2\cos^2\varphi+a_0^2\sin^2\varphi)^{1/2}$. The exact stream lines (28) have a bend (discontinuity in their slope) in the penetrated region on the x axis at $a(b)<|x|<a_0-b_0^2/a_0$, but they are smooth at $a_0-b_0/a_0^2\leqslant|x|\leqslant a_0$. Our approximate solution coincides with these exact stream lines within line thickness.

From the stream lines in the critical state, Eq. (28), one obtains the exact magnetic moment of thin ellipses in the fully penetrated critical state,

$$m_{\rm sat}^{\rm exact}=-\frac{4}{3}J_c a_0 b_0^2\left[E(k)-\frac{e^2}{2}K(k)\right], \tag{29}$$

where $K(k)$ and $E(k)$ are the elliptic integrals of the first and second kind with $k^2=1-e^2$, $e=b_0/a_0$, see the Appendix. Comparing the exact result (29) with our approximate $m_{\rm sat}$, Eq. (24), we find that the deviation is extremely small.

Writing $f_1(e)=\cos(e\pi/2)/(1-e^2)$ and $f_2(e)=E(k)-(e^2/2)K(k)$ we find $f_1(1)=f_2(1)=\pi/4$ (disk), $f_1(0)=f_2(0)=1$ (strip), and $0\leqslant f_1-f_2\leqslant 0.001\,317$. The maximum deviation $f_1-f_2=0.001\,317$ occurs at $e=0.5043$. The deviation is an almost symmetric function of the eccentricity e, $f_1(e)-f_2(e)\approx 0.001\,38\sin^2(e\pi)$. With Eq. (29) the field H_1 (25) which enters formula (26) takes the exact value

$$H_1^{\rm exact}=\frac{m_{\rm sat}^{\rm exact}}{m'(0)}=H_cE(k)\left[E(k)-\frac{e^2}{2}K(k)\right]. \qquad (30)$$

The flux fronts, current stream lines, and contour lines of the magnetic field $H_z(x,y)$ in the general elliptic film do not coincide, as opposed to the situation in circular disks, long strips, and in longitudinal geometry. These features of the critical state in noncircular thin superconductors of finite size are seen even more clearly in square and rectangular films,[9–11] but while those geometries were solved numerically, we now have an analytic solution for the elliptic film.

Another feature of the critical state in thin elliptic films as compared to the critical state in circular disks and infinite strips, is that the *direction* of the sheet current **J** at a given point (x,y) *changes* during the penetration of flux, see Fig. 7. This fact may have an important physical consequence for films or platelets with thickness exceeding the London penetration depth λ. As is known,[12–16] in flat superconductors with $d\gg\lambda$ in moderate fields H there is a flux and current-free core described by $|z|<z_{\rm core}(x,y)$. In the cases of strips and disks this core was depicted, e.g., in Refs. 13,16. Critical currents circulate only outside the core, for $z_{\rm core}(x,y)<|z|<d/2$. In this shell the critical state has the usual Bean form, but the field gradient occurs *across the thickness* of the sample since this state is forced by the screening currents, and the flux lines are almost *parallel* to the flat surface. The outer rim (equator) of the flux-free core coincides with the penetrating flux front since in the region inside the flux front the perpendicular magnetic field B_z is practically zero.

Now, since the tangential field at the flat surface is perpendicular to the sheet current **J**, the changing direction of $\mathbf{J}(x,y;b)$ during flux penetration (i.e., with increasing H and decreasing b) means that the direction of the penetrating flux lines in the region below γ also changes. Thus, flux lines *with gradually rotating orientation* enter through the flat surface at each point away from the symmetry axes. These U-shaped flux lines move towards the specimen center, dragged by the Lorentz force, which is balanced by bulk pinning. As a result, in the region inside γ the layers of the flux-line lattice exhibit torsion relative to each other and therefore carry a longitudinal current component, i.e., the local current density is not exactly perpendicular to the flux lines. In principle, this may lead to instabilities and flux-cutting processes.[17–19] That situation may be related to the penetration of a rotating field component discussed by Bean[20] and by Gilchrist.[21]

In deriving the solution we have assumed that $\mathbf{B}=\mu_0\mathbf{H}$ and the so-called geometrical barrier[22–25] is negligible. These assumptions hold if the characteristic magnetic field j_cd considerably exceeds the lower critical field H_{c1}. In the case $j_cd<H_{c1}$ and $H<H_{c1}$ the critical state problem becomes more complicated. Analytical[22,23] and numerical[24,25] methods to analyze this general problem were recently proposed. In particular, if our assumption $\mathbf{B}=\mu_0\mathbf{H}$ is replaced by the correct $H(B)$ (obtained, e.g., from Ginzburg-Landau theory[26]) then flux does not penetrate until the applied field H has reached the field of first penetration of flux, $H_{en}\approx H_{c1}\tanh\sqrt{cd/2w}$, where $c\approx0.36$ for strips with half width w and $c\approx0.67$ for disks with radius w.[25]

IV. ANISOTROPIC CRITICAL CURRENT

The obtained solution allows one to analyze the critical state of flat superconductors when the critical current density j_c is *anisotropic* in the plane of the film. Such anisotropy can occur, for example, if there are twin boundaries or other extended or inclined defects, or if the superconductor itself is anisotropic. A controlled in-plane anisotropy of j_c of more complicated nature may be induced by applying a magnetic field parallel to the film.[27] To explain our analysis, we perform a transformation of coordinates:

$$x=\alpha x', \qquad y=\beta y', \qquad (31)$$

where α and β are some constants and the prime denotes the transformed quantities. Under this transformation the ellipse with semiaxes a_0 and b_0 goes over to an ellipse with semiaxes $a_0'=a_0/\alpha$, $b_0'=b_0/\beta$, while any small line element, dl, directed at an angle φ relative to the x axis, is transformed into the element

$$dl'=dl\left(\frac{\cos^2\varphi}{\alpha^2}+\frac{\sin^2\varphi}{\beta^2}\right)^{1/2},$$

which is directed at an angle φ' with

$$\tan\varphi'=\frac{\alpha}{\beta}\tan\varphi.$$

Since the current crossing the line element must be invariant, we obtain the following transformation of the sheet current flowing at an angle $\psi=\varphi\pm\pi/2$ relative to the x axis:

$$J'(\psi')=J(\psi)\beta\left[1+\left(\frac{\alpha^2-\beta^2}{\beta^2}\right)\sin^2\psi'\right]^{1/2}.$$

Thus, if the anisotropic critical current density in some elliptic sample with semiaxes a_0', b_0' can be approximated by the expression

$$J_c'(\psi')=\text{const}(1+\delta\sin^2\psi')^{1/2}, \qquad (32)$$

in which δ is some constant ($\delta>-1$), we may reduce the critical state problem of this anisotropic sample to the isotropic problem by performing the transformation (31) from x', y' to x, y with $\beta=1$ and $\alpha=\sqrt{1+\delta}$. After the transformation we shall have an elliptic sample with semiaxes $a_0=\sqrt{1+\delta}a_0'$, $b_0=b_0'$ and with isotropic critical current $J_c=\text{const}$, and we can use the solution obtained in Sec. II.

Thus, our solution permits to analyze (at least qualitatively) the features of the critical state of anisotropic superconducting films. For example, for a circular disk with radius R and with anisotropic critical current obeying Eq. (32) with $\delta=1$, one obtains the transformed ellipse with semiaxes $a_0=\sqrt{2}R$, $b_0=R$ and the current distribution and stream lines depicted in Figs. 4–7 for $e=0.7$, and the magnetic field depicted in Figs. 9 and 10. These pictures then are transformed back to the coordinates of the original circular disk by shrinking them along x by a factor of 0.7. Figure 12 shows another example of a circular disk with larger anisotropy $\delta=3$, yielding $J_c(\pi/2)/J_c(0)=a_0/b_0=2$. The results of Ref. 27 for square and rectangular plates with anisotropic critical current are in agreement with this approach. Our solution may also be used to include the in-plane anisotropy of the

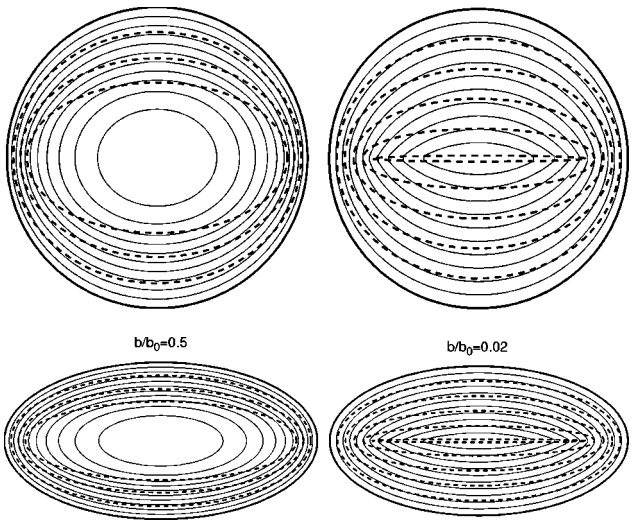

FIG. 12. Current stream lines (solid curves) and flux fronts (dashed curves) in a circular disk with anisotropic critical current density, $J_{cy}/J_{cx}=J(\pi/2)/J_c(0)=2$ [$\delta=3$ in Eq. (32)] for half ($b/b_0=0.5$, left) and full ($b/b_0=0.02$, right) penetration of flux. Shown at the bottom is the isotropic ellipse with axis ratio $b_0/a_0=0.5$ to which this problem transforms. This ellipse exhibits equidistant current stream lines outside the inner flux front.

critical current into theories[14,15] which analyze the critical state in flat superconductors taking into account the current anisotropy (**B**/B dependence) associated with the curvature of the flux lines.

V. CONCLUSION

In this paper we derived an approximate analytic solution of the Bean critical-state model for thin elliptic superconductors with semiaxes a_0 and $b_0=ea_0$ in a perpendicular field H. The accuracy of this solution is high and the known limiting cases of a circular disk and a long strip are recovered exactly. With increasing H the penetrating flux front is an ellipse with axes a and b related by Eq. (13) such that at full penetration, when $b=0$, $a(b)$ stays finite, i.e., there is a section of length $2a(0)=2a_0\cos(\pi e/2)$ on the x axis where regions with different orientation of the current meet, similar to the situation in rectangular platelets.[9,11,27] The current stream lines in the penetrated region deviate from ellipses and, in the fully penetrated state, they have a sharp bend on the x axis in the interval $|x|\leq a_0-b_0^2/a_0$ that is slightly wider than $2a(0)$.

Our analytic solution shows that in noncircular finite superconductor films at any point not located near a symmetry axis or near the edge, when H is increased the direction of the circulating sheet current changes until the flux front passes through this point, see Fig. 7. Therefore, in samples with thickness d exceeding the London penetration depth λ, the orientation of the flux lines penetrating from the two flat surfaces changes also, since at the flat surfaces the flux lines are at a right angle to the sheet current. As a consequence, the flux-line arrangment rotates along z in the region where $B_z=0$. Furthermore, it cannot be ruled out that also in the region with $B_z\neq 0$ the flux lines are twisted, i.e., their curvature is not planar. If this twist occurs, it means that the orientation of the current at fixed x,y but different depth z varies, and the integrated current density $J(x,y)$ is not necessarily equal to j_cd or exactly constant even in the flux-penetrated region. The precise calculation of the flux and current distributions inside noncircular disks even of *small* thickness $d>\lambda$ then becomes an intricate 3D problem. The possibility of twisted flux lines in the penetrated region of noncircular thin disks should thus be considered in more detail in future work.

ACKNOWLEDGMENT

We gratefully acknowledge stimulating discussions with John Gilchrist.

APPENDIX: EVALUATION

The integrals (11) for H/H_c, Eq. (18) for $H_z(x,y)$, and Eq. (19) for J_x, J_y, and $g(x,y)$, like the elliptic integral of the second kind,

$$E(\varphi,k)=E(s,m)=s\int_0^1\sqrt{\frac{1-ms^2t^2}{1-s^2t^2}}dt \qquad \text{(A1)}$$

with $s=\sin\varphi$, $m=k^2$, may be evaluated with high precision by a substitution of variables. We first transform the integrals over b' into integrals over a variable t in the interval $0\leq t\leq 1$, like Eq. (A1). Noting that these integrands may have poles $\propto 1/\sqrt{t}$ and $\propto 1/\sqrt{1-t}$ at the boundaries, we use a substitution

$$I=\int_0^1 f(t)dt=\int_0^1 f[t(u)]t'(u)du, \qquad \text{(A2)}$$

which has a weight function $t'(u)=dt/du$ that vanishes with a high power of u and $1-u$ at $u=t=0$ and at $u=t=1$. A good such choice is

$$t=g(u)=35u^4-84u^5+70u^6-20u^7$$

$$t'=g'(u)=140u^3(1-u)^3. \qquad \text{(A3)}$$

An even better choice is to iterate Eq. (A3) once, writing

$$t=g[g(u)], \qquad t'=g'(u)g'[g(u)]. \qquad \text{(A4)}$$

With Eq. (A4) one has $t\propto u^{16}$ and $t'\propto u^{15}$ near $t=0$, and $1-t\propto(1-u)^{16}$ and $t'\propto(1-u)^{15}$ near $t=1$. The pole $f(t)\propto 1/\sqrt{t}$ in the original integrand is now removed in the substituted integrand $F(u)=f[t(u)]\,t'(u)\propto u^7$ and similarly near $t=1$. Since the integrand vanishes rapidly at the boundaries of the integral, one may use an integration method with constant weights,

$$I=\int_0^1 F(u)du\approx\frac{1}{N}\sum_{i=1}^{N}F\left(\frac{i-1/2}{N}\right). \qquad \text{(A5)}$$

This method achieves high precision $\approx 10^{-8}$ even with a small grid number $N=20$–30.

In Eqs. (11), (14), etc., $E(k)$ is given by the definition (A1) with $s=1$, and for $K(k)$ in Eq. (29) a similar definition applies. All these elliptic integrals are easily computed with high accuracy by this integration method.

Before the integrals for $H_z(x,y)$ and $g(x,y)$ can be evaluated for a 2D grid of points (x,y), one has to find the elliptic flux front that passed through the point (x,y). This may be done by finding the zeros of the function

$$p(b_{xy}) = \frac{x^2}{a_{xy}^2} + \frac{y^2}{b_{xy}^2} - 1$$

with $a_{xy} = \cos[b_0 \arccos(b_{xy}/b_0)]$, cf. Eqs. (13) and (17) with length unit $a_0 = 1$. This is achieved by starting with $b_{xy} = b$ (the short semiaxis of the inner flux front) and iterating $b_{xy} \leftarrow b_{xy} - 2\epsilon p(b_{xy})/[p(b_{xy}+\epsilon) - p(b_{xy}-\epsilon)]$ ($\epsilon \ll 1$) a few times. A similar procedure may be used to invert the relation $H(b)$, Eq. (11), to obtain $b(H)$. To obtain the correct $g(x,y)$ also inside the flux front, and $H_z(x,y)$ also outside the superconductor, we chose $b_{xy} = b_0$ for all points outside the ellipse with semiaxes a_0, b_0, and $b_{xy} = b$ for all points inside the ellipse with semiaxes a, b by putting $b_{xy} \leftarrow \max[b, \min(b_{xy}, b_0)]$.

[1] E. H. Brandt, Rep. Prog. Phys. **58**, 1465 (1995).
[2] P. N. Mikheenko and Yu. E. Kuzovlev, Physica C **204**, 229 (1994).
[3] E. H. Brandt, M. V. Indenbom, and A. Forkl, Europhys. Lett. **22**, 735 (1993).
[4] E. H. Brandt and M. V. Indenbom, Phys. Rev. B **48**, 12 893 (1993).
[5] E. Zeldov, J. R. Clem, M. McElfresh, and M. Darwin, Phys. Rev. B **49**, 9802 (1994).
[6] L. D. Landau and E. M. Lifshitz, *Electrodynamics of Continuous Media*, Course in Theoretical Physics Vol. 8 (Pergamon, London, 1959).
[7] J. A. Osborn, Phys. Rev. **67**, 351 (1945).
[8] E. H. Brandt, Phys. Rev. B **46**, 8628 (1992).
[9] E. H. Brandt, Phys. Rev. B **52**, 15 442 (1995); Phys. Rev. Lett. **74**, 3025 (1995).
[10] L. Prigozhin, J. Comput. Phys. **144**, 180 (1998).
[11] Th. Schuster, H. Kuhn, E. H. Brandt, M. V. Indenbom, M. Leghissa, M. Kraus, M. Kläser, G. Müller-Vogt, H.-U. Habermeier, H. Kronmüller, and A. Forkl, Phys. Rev. B **52**, 10 375 (1995).
[12] D. J. Frankel, J. Appl. Phys. **50**, 5402 (1972).
[13] E. H. Brandt, Phys. Rev. B **54**, 4246 (1996).
[14] I. M. Babich and G. P. Mikitik, Phys. Rev. B **54**, 6576 (1996).
[15] I. M. Babich and G. P. Mikitik, Phys. Rev. B **58**, 14 207 (1998).
[16] E. H. Brandt, Phys. Rev. B **58**, 6506 (1998).
[17] A. M. Campbell and J. E. Evetts, Adv. Phys. **72**, 199 (1972).
[18] J. R. Clem, Phys. Rev. Lett. **24**, 1425 (1977); J. Low Temp. Phys. **38**, 353 (1980); Physica B **107**, 453 (1981); A. Perez-Gonzalez and J. R. Clem, Phys. Rev. B **43**, 7792 (1991).
[19] E. H. Brandt, Phys. Lett. **79A**, 207 (1980); J. Low Temp. Phys. **39**, 41 (1980); E. H. Brandt, **4**, 33 (1981); **44**, 59 (1981).
[20] C. P. Bean, J. Appl. Phys. **41**, 2482 (1970).
[21] J. Gilchrist, J. Phys. D **5**, 2252 (1972); Supercond. Sci. Technol. **3**, 93 (1990); **7**, 849 (1994).
[22] E. Zeldov, A. I. Larkin, V. B. Geshkenbein, M. Konczykowski, D. Majer, B. Khaykovich, V. M. Vinokur, and H. Strikhman, Phys. Rev. Lett. **73**, 1428 (1994).
[23] M. Benkraouda and J. R. Clem, Phys. Rev. B **53**, 5716 (1996); N. Morozov *et al.*, Physica C **291**, 113 (1997); A. V. Kuznetsov *et al.*, Phys. Rev. B **56**, 9064 (1997).
[24] R. Labusch and T. B. Doyle, Physica C **290**, 143 (1997); T. B. Doyle, R. Labusch, and R. A. Doyle, *ibid.* **290**, 148 (1997).
[25] E. H. Brandt, Phys. Rev. B **59**, 3369 (1999).
[26] E. H. Brandt, Phys. Rev. Lett. **78**, 2208 (1997).
[27] Th. Schuster, H. Kuhn, E. H. Brandt, and S. Klaumünzer, Phys. Rev. B **56**, 3413 (1997).